A Determination Method of Rainfall Type Based on Rainfall-Induced Slope Instability

Yafen ZHANG
Open University of China
Yulong ZHU (zhuyulong@ncepu.edu.cn)
North China Electric Power University https://orcid.org/0000-0002-7149-9377
Xiaoyu YAN
Open University of China
Shu LI
Open University of China
Qijing YU
Open University of China
Yidan WANG
Open University of China

Research Article

Keywords: Rainfall types, SH type rainfall, LL type rainfall, Slope instability, intensity-duration (I–D) conditions

Posted Date: December 13th, 2021

DOI: https://doi.org/10.21203/rs.3.rs-1148172/v1

Version of Record: A version of this preprint was published at Natural Hazards on March 11th, 2022. See the published version at https://doi.org/10.1007/s11069-022-05301-2.

Abstract

This work presents a determination method of rainfall types based on rainfall-induced slope instability to eliminate the current dilemma of the inconsistent classification of rainfall types. Firstly, 5,808 scenarios of slope instability are simulated with 11 kinds of soil properties under 528 designed intensity-duration (I–D) conditions. Then through analysis of the I–D conditions when slope failure occurred, rainfall is classified into two types: short-duration – high-intensity (SH) type, and long-duration – low-intensity (LL) type. According to the analysis results, it indicates that rainfall types affect the initiation of slope failure, i.e., different I–D conditions will affect the slope failure initiation under LL type rainfall, while the slope failure initiation will not be affected by the change of I–D conditions under SH type rainfall. In addition, the results show that the classification of rainfall types does not depend on the soil shear strength parameters (cohesion and internal friction angle), although the change of soil shear strength parameters will cause the shift of threshold curve of slope failure in the I–D conditions two-dimensional (2D) plane. The findings in this study benefit to understanding the effect of rainfall type on the mechanism of slope failure initiation, which will promote the development of an early warning system of slope failure in the future by considering the identification of rainfall types.

Highlights

1. Rainfall can be classified into SH type and LL type.
2. Classification of rainfall types does not depend on soil shear strength parameters.
3. Rainfall types affect the initiation of slope failure.

1. Introduction

Rainfall is considered a key factor for triggering slope failure, and more than thousands of rainfall-induced slope failures occur around the world every year (Rahardjo et al., 2005; Zhang et al., 2014; Van Asch et al., 2018; Zhu et al., 2020a). Particularly, the different rainfall conditions/types cause slope failure to occur in different patterns, for example, heavy rainfall like rainstorms or torrential rain will make the surface layer of the soil saturated in a short time (Zhu et al., 2020b). The pore air between the saturated surface layer and the phreatic layer is enclosed in the soil, thereby preventing the downward infiltration of water. In this case, the water that has not infiltrated into the soil produces runoff on the ground surface, which will cause erosion of the ground surface and cause shallow slope failure/landslides (Larsen and Simon, 1993). On the other hand, during light rain, the weak rainfall intensity will not quickly saturate the surface layer of the soil. This makes it difficult to create the closed region of pore air. The infiltrated water replaces the pore air in the soil, and the pore air is expelled from the soil through the soil surface (Kuang et al., 2013). Accordingly, water can continuously infiltrate into the deep soil layer, resulting in the continuous increase of the water content in the deep soil layer, thereby reducing the matric suction and subsequently inducing the occurrence of deep-seated slope failure/landslide (Larsen and Simon, 1993).

Therefore, it cannot be ignored that the type of rainfall has a significant influence on the infiltration behavior of soil moisture and the failure pattern of the slope.

In the past few decades, many scholars have made great efforts to establish the link between rainfall and slope instability (e.g., Larsen and Simon, 1993; Guzzetti et al., 2008; Saito et al., 2010; Segoni et al., 2014; Chen et al., 2015; Guo et al., 2016; Abraham et al., 2020; Marin et al., 2021; Kim et al., 2021). A considerable part of their research focuses on a widely used method, namely intensity-duration (I–D) threshold models, as the I-D threshold is considered an effective indicator for rainfall-induced slope failure/landslides (Kim et al., 2021). Among them, the most famous one is the power function of rainfall intensity as rainfall duration (i.e., $I=aD^b$, I is rainfall intensity; D is rainfall duration; a and b are fitting parameters). For example, Marin et al., (2021) evaluated the applicability of the two methods (physically-based model and observed landslides) to define rainfall I-D thresholds in individual basins and emphasized the merits of both methods. Abraham et al. (2020) pondered the effect of the selection of rainfall parameters for developing a regional scale rainfall threshold in a data-sparse region and pointed out that the approach selecting the rain gauge based on the most extreme rainfall parameters performed better than the other approaches. However, the main focus of discussion in these studies is the method of the determination of the rainfall intensity, i.e., the average rainfall intensity (Saito et al., 2010), the peak rainfall total (Jarosińska, 2018), or the antecedent rainfall (Kim et al., 2021).

For the rainfall types, the concepts of short-duration – high-intensity (SH) type and long-duration – low-intensity (LL) type have been mentioned in many studies (Chen et al., 2015; Perera et al., 2017; Deng et al., 2018; Jin et al., 2021; Marin et al., 2021; Kim et al., 2021), but almost all judgments are arbitrary or subjective. For example, Jin et al. (2021) defined the rainfall event (I=25 mm/h and D=8 h) as SH type rainfall and the rainfall event (I=0.4 mm/h and D=168 h) as LL type rainfall. Otherwise, the criteria for classifying rainfall types are not uniform. For example, Chen et al. (2015) set the criteria of SH type rainfall as short-duration (<2 h) and high-intensity (>16.1 mm/h) and the criteria for LL type rainfall as long-duration (>71 h) and low-intensity (<8.8 mm/h). While Perera et al. (2017) set the criteria of SH type rainfall as short-duration (<2 h) and high-intensity (>54 mm/h) and the criteria for LL type rainfall as long-duration (>8 h) and low-intensity (<25 mm/h). Apart from the above studies, Saito et al. (2010) examined rainfall I-D conditions of 1,174 shallow landslides that occurred during 2006–2008 in Japan and classified the rainfall type into SH type and LL type based on statistical results as shown in Fig. 1. However, from Fig. 1(b), it can be seen that the criterion for classifying rainfall types proposed by Saito et al. (2010) is too small. The main reason may be that the object of investigation in the study of Saito et al. (2010) is shallow landslides, which are usually induced by heavy rainfall or the erosion of the surface caused by long-term light rain.

Therefore, to eliminate the current dilemma of the inconsistent classification of rainfall types, this study attempts to present a determination method of rainfall type based on rainfall-induced slope instability. Through the analysis of the I–D conditions corresponding to 4,752 scenarios of slope instability, and subsequently, according to the effect of rainfall types on the initiation of slope failure, a determination method of rainfall type (SH type and LL type) based on rainfall-induced slope instability is proposed.

2. Methods

2.1 Governing equation of seepage flow

The governing equation for two-dimensional seepage flow is as given by Richards, (1931) and Childs and Collins-George, (1950),

$$\frac{1}{\rho_w}\frac{\partial}{\partial x}\left(D_v\frac{\partial P_v}{\partial x}\right)+\frac{1}{\rho_w}\frac{\partial}{\partial y}\left(D_v\frac{\partial P_v}{\partial y}\right)+\frac{\partial}{\partial x}\left(k_x\frac{\partial\left(\frac{P}{\rho_w g}+y\right)}{\partial x}\right)+\frac{\partial}{\partial y}\left(k_y\frac{\partial\left(\frac{P}{\rho_w g}+y\right)}{\partial y}\right)+Q=m_w\frac{\partial P}{\partial t} \qquad (1)$$

where, ρ_w is density of water (kg/m^3); D_v is diffusion coefficient of water vapor through soil ((kg•m)/(kN•s)); P_v is vapor pressure of soil moisture (kPa); y is elevation (m); P is pressure (kPa); k_x, k_y is hydraulic conductivity in the x-direction and y-direction (m/s), respectively; g is gravity acceleration (9.81 m/s^2); Q is boundary flux (1/s); m_w is slope of the soil water characteristic curve, SWCC (1/kPa); γ_w is unit weight of water (kN/m^3) and t is time (s).

2.2 Shear strength of unsaturated soil

The shear strength of unsaturated soil is expressed based on Bishop's effective stress principle as given by Vanapalli et al. (1996),

$$\tau = c' + (\sigma_n - u_a)\tan\ \phi' + (u_a - u_w)\left[\frac{\theta_w-\theta_r}{\theta_s-\theta_r}\tan\ \phi'\right] \qquad (2)$$

where, τ is the shear strength of unsaturated soil (kPa); c' is the effective cohesion (kPa); ϕ' is the effective angle of internal friction (°); u_a is the pore air pressure (kPa); u_w is the pore water pressure (kPa); σ_n is net total stress (kPa); θ_w is volumetric water content (m^3/m^3); θ_s is saturated volumetric water content (m^3/m^3) and θ_r is residual volumetric water content (m^3/m^3).

2.3 Slope stability analyzed by limit equilibrium method

Slope stability has been analyzed using the limit equilibrium method given by Morgenstern and Price (1965),

$$F_m = \frac{\sum[c'lR+\{N-u_w l\chi-u_a l(1-\chi)\}R\tan\ \phi']}{\sum Wx-\sum Nf} \qquad (3)$$

where, W is the total weight of a slice as shown in Fig. 2 (kN); N is the total normal force on the base of the slice (kN); x is the horizontal distance from the centerline of each slice to the center of rotation (m); f is the perpendicular offset of the normal force from the center of rotation (m); R is the radius of a circular slip surface (m); l is the base length of each slice (m); χ is a parameter related to the degree of saturation, $\chi=(\theta_w-\theta_r)/(\theta_s-\theta_r)$. The Morgenstern and Price Method (Fig. 2) considers both shear (X) and normal (E) interslice forces and satisfies both moment and force equilibrium (Morgenstern and Price, 1965).

2. Numerical Model And Materials

A 2D homogeneous conceptual slopes model is established to simulate slope stability under different I-D conditions by using the general software package, GeoStudio (GeoStudio, 2007). Fig. 3 shows the size of the numerical model and the applied boundary conditions. During the simulation, rainfall data is applied on the soil surface (ab, bc, cd in Fig. 3) and no flow boundary is applied on the left side (af in Fig. 3), right side (de in Fig. 3), and bottom side (ef in Fig. 3) of the model. The initial groundwater level (GWL) is set as -3m (blue dash line in Fig. 3) and the stable GWL is the simulated GWL after the initial steady-state analysis (red dash line in Fig. 3). The slope height (H) is assumed as 10 m and the slope angle (α) is assumed as 45°.

The soil properties are given as a kind of volcanic ash distributed in Hokkaido, Japan as listed in Table 1. Dry density (ρ_d), porosity (n), effective cohesion (c'), effective internal friction angle (ϕ'), and saturated hydraulic conductivity (k_s), were measured by Sato et al. (2017). Fig. 4 shows the soil-water characteristic curve (SWCC) and hydraulic conductivity of the soil. The SWCC of the slope is estimated from the grain size distribution curve by referring to Fredlund et al., (2002). The hydraulic conductivity of the soil is estimated based on the SWCC through the estimator in GeoStudio (GeoStudio, 2007).

Table 1
Soil properties used for the simulation.

Parameters	Value
Dry density, ρ_d (kg/m^3)	1695
Porosity, n (1)	0.36
Effective cohesion, c' (kPa)	0
Effective friction angle, ϕ' (°)	35
Saturated hydraulic conductivity, k_s (m/s)	1.12×10^{-5}
Saturated volumetric water content, θ_s (m^3/m^3)	0.36
Residual volumetric water content, θ_r (m^3/m^3)	0.035
van Genuchten parameter, α (1/m)	0.538
van Genuchten parameter, m	0.468

There are 22 different rainfall intensities and 24 different rainfall duration are designed as listed in Table 2. Therefore, a total of 528 kinds of I-D conditions have been designed. The minimum rainfall intensity is set to 10 mm/h, and the maximum rainfall intensity is set to 60 mm/h. The intensity of the rest rainfall increases in increments of 2 mm/h. It is worth noting that the rainfall intensity in this study means the average rainfall intensity, i.e., within the rainfall duration, the design intensity is a constant value.

Table 2
Different designed I-D conditions.

	Designed I-D conditions										
Rainfall intensity (mm/h)	10	12	14	16	18	20	22	24	26	28	30
Rainfall duration (h)	0-24	0-24	0-24	0-24	0-24	0-24	0-24	0-24	0-24	0-24	0-24
Rainfall intensity (mm/h)	32	34	36	38	40	42	44	46	48	50	60
Rainfall duration (h)	0-24	0-24	0-24	0-24	0-24	0-24	0-24	0-24	0-24	0-24	0-24
Total number	22 different rainfall intensities × 24 different rainfall duration = 528										

4. Results

4.1 slope instability under different I-D conditions

Two different approaches can be selected to simulate the gradual progress of the slope from stable to unstable. One way is to keep the rainfall duration constant and gradually increase the rainfall intensity, while the other way is to keep the rainfall intensity constant and gradually extend the rainfall duration. Due to under the same rainfall intensity, with the increase in the rainfall duration, the stability of the slope will continue to decline, i.e., the factor of safety (FOS) of the slope will gradually decrease. This makes it much easier to capture the process of slope from stable to failure, so the second approach is used in this study. Fig. 5 shows part of the simulation results (c'=3 kPa, ϕ'=35°) of the slope stability under different I-D conditions. Fig. 5 suggests that under low rainfall intensity, the stability of the slope drops very smoothly. However, it is worth noting that in the case of weak rainfall, as the rainfall intensity increases, the FOS curve will become steeper. While, when the rainfall intensity increases to a certain degree, even if the rainfall intensity further increases, the stability of the slope does not change significantly as shown from Fig. 5(g) to Fig. 5(i).

The I-D conditions when the slope failure occurs (FOS is less than 1.0 for the first time) are screened out and plotted in Fig. 6. From Fig. 6, it can be recognized that the threshold curve formed by the simulation results conforms to the rule in the wide-used early warning system that the rainfall intensity is the power

function of the rainfall duration. This implies that the calculation results are reliable and effective. However, it should be noted that a very interesting phenomenon was discovered as described in the previous paragraph, the increase in rainfall intensity will advance the time of slope failure, but when the rainfall intensity exceeds 32 mm/h (in the case discussed in this study), the slope failure time will no longer change even if the rainfall intensity continues to increase.

4.2 slope instability under different soil properties

To investigate whether the finding in Section 4.1 is an accidental phenomenon caused by an unreasonable model setting or an objective law that prevails in reality, 11 kinds of soil properties with different cohesion (0 kPa, 1 kPa, 2 kPa, 3 kPa, 4 kPa, and 5 kPa) and internal friction angle (33°, 34°, 35°, 36°, 37°, and 40°) as listed in Table 3 were discussed. In the simulation, the controlled variable method is used, that is, when the cohesion changes, the internal friction angle remains constant (ϕ' = 35°), and when the internal friction angle changes, the cohesion remains constant (c'= 0 kPa).

Table 3
Different designed soil properties.

	Designed soil properties					
Different cohesion (ϕ' = 35°) (cohesion (kPa)/internal friction angle (°))	0/35	1/35	2/35	3/35	4/35	5/35
Different internal friction angle (c'= 0 kPa) (cohesion (kPa)/internal friction angle (°))	0/33	0/34	–	0/36	0/37	0/40
Total number	11 kinds of soil properties					

A total of 5,808 scenarios of slope instability are simulated with 11 kinds of soil properties under 528 designed intensity-duration (I–D) conditions. Fig. 7 and Fig. 8 show the threshold curves formed by the occurrence points of slope failure (FOS is less than 1.0 for the first time) under the variation of cohesion and the variation of internal friction angle, respectively. From Fig. 7, it shows that the change of cohesion will cause the obvious rightward shift of the threshold curve of slope failure in the I–D conditions 2D plane no matter under relatively heavy rainfall or relatively weak rainfall. The difference is that under relatively heavy rainfall conditions, the threshold curve of slope failure moves to the right nearly parallel to the x-axis in the I–D conditions 2D plane, while under relatively weak rainfall conditions, the threshold curve of slope failure moves to the upper right at a certain angle to the x-axis in the I–D conditions 2D plane. In addition, Fig. 8 shows that the effect of the change of internal friction angle on the threshold curve of slope failure. From Fig. 8, it can be identified that under relatively heavy rainfall conditions, there is no obvious movement of the threshold curve of slope failure was observed in the I–D conditions 2D plane, while under relatively weak rainfall conditions, although the magnitude of the movement is not as obvious as in Fig. 7, the trend of the threshold curve of slope failure moving towards the upper right at a certain angle to the x-axis in the I–D conditions 2D plane still can be recognized.

From the overall analysis of Fig. 7 and Fig. 8, the results show that no matter under different cohesion conditions or different internal friction angle conditions, when the rainfall intensity exceeds a certain value, i.e, critical intensity (I_C), the occurrence time of slope failure will no longer be advanced even if the rainfall intensity continues to increase. Furthermore, the critical intensity (I_C) is not affected by the variation in cohesion and internal friction angle, for example, in all 11 kinds of soil properties, the value of the critical intensity (I_C) is about 32 mm/h (in the case discussed in this study).

4.3 Proposal of the determination method of rainfall types

Indeed, two rainfall intensities (high/low intensity) and two rainfall duration (short/long duration) can be combined into four rainfall types: short-duration – high-intensity (SH) type, short-duration – low-intensity (SL) type, long-duration – high-intensity (LH) type, and long-duration – low-intensity (LL) type. However, the stability of the slope will not be significantly reduced under SL type rainfall, as rainfall intensity is very low and its duration is also short, i.e., the rainfall conditions are in a safe zone. While, under LH type rainfall, a large number of slope failures will occur with a high probability. In this case, the rainfall conditions are in a dangerous zone. The applicability of the early warning system in these two situations is very low, so the discussion is concentrated on SH type rainfall and LL type rainfall because in these two cases, the slope changes from stable to failure.

Combining the findings of Section 4.1 and Section 4.2, through analysis of 5,808 scenarios of slope instability with 11 kinds of soil properties under 528 designed intensity-duration (I–D) conditions, using geometric methods, rainfall is classified into two types: short-duration – high-intensity (SH) type, and long-duration – low-intensity (LL) type as shown in Fig. 9 (a) and Fig. 9(b). The red solid line in Fig. 9(a) and Fig. 9(b) is the outer boundary line of SH type rainfall and LL type rainfall, namely critical duration (D_c), and the blue solid line in Fig. 9(a) and Fig. 9(b) is the inner boundary line of SH type rainfall and LL type rainfall, namely critical intensity (I_c). It is worth noting that the inner boundary line (purple solid line) of SH type rainfall and LL type rainfall proposed by Saito et al. (2010) is too small.

Accordingly, a new determination method of rainfall types (SH type rainfall and LL type rainfall) is proposed as shown in Fig. 10. The expression is as follow,

$$\begin{cases} D_L \le D \le D_U & ,if \quad I \ge I_C \quad \text{SH type rainfall} \\ \frac{I_c - I}{tan\beta} + D_L \le D \le \frac{I_c - I}{tan\beta} + D_U & ,if \quad I < I_C \quad \text{LL type rainfall} \end{cases} \tag{4}$$

where, D_L is the lower limit of rainfall duration (h); D_U is the upper limit of rainfall duration (h); β is a slope angle between 0 and 90°. That is if the average rainfall intensity (I) exceeds the critical intensity (I_c), the rainfall duration between D_L and D_U is SH type rainfall, i.e., rainfall conditions are located in the light green rectangle zone in Fig. 10. If the average rainfall intensity (I) does not exceed the critical intensity (I_c) and the rainfall duration is in the light blue diamond-shaped zone surrounded by critical duration (D_c) and critical intensity (I_c) in Fig. 10, it is LL type rainfall.

From Fig. 9 and Fig. 10, the results show that the classification of rainfall types does not depend on the soil shear strength parameters, although the change of soil shear strength parameters will cause the shift of threshold of slope failure in the I–D conditions two-dimensional (2D) plane. The main reason is that although the cohesion and internal friction angle are the controlling factors of soil shear strength, under rainfall conditions, it is the soil volumetric water content (matric suction) that plays a key role in the stability of the slope. Meanwhile, the type of rainfall is the main factor affecting the change of soil volumetric water content in the slope.

5. Conclusions

This work simulated 5,808 scenarios of slope instability with 11 kinds of soil properties under 528 designed intensity-duration (I–D) conditions. Then through analysis of the I–D conditions when slope failure occurred, a determination method of rainfall types (SH type rainfall and LL type rainfall) is proposed. According to the analysis results, it indicates that rainfall types affect the initiation of slope failure, that is in the case of LL type rainfall, the increase in rainfall intensity will advance the time of slope failure. While, in the case of SH type rainfall, i.e., when the rainfall intensity exceeds the critical intensity (I_c), even if the rainfall intensity further increases, the stability of the slope does not change significantly, i.e., the occurrence time of slope failure will no longer change.

In addition, under LL type rainfall, the change of cohesion and internal friction angle will make the threshold curve of slope failure to move towards the upper right at a certain angle to the x-axis in the I–D conditions 2D plane. While under SH type rainfall, the change of cohesion will make the threshold curve of slope failure to move towards the right nearly parallel to the x-axis in the I–D conditions 2D plane, but the effect of changes in internal friction angle is not obvious. Furthermore, the classification of rainfall types only depends on the relationship between the rainfall intensity (I) and critical intensity (I_c) and the relationship between the rainfall duration (D) and critical duration (D_c). It does not depend on the soil shear strength parameters (cohesion and internal friction angle).

The findings in this study will benefit to understand the effect of rainfall type on the mechanism of slope failure initiation, which will promote the development of an early warning system of slope failure in the future by considering the identification of rainfall types.

Declarations

Acknowledgments

This work was financially supported by the Fundamental Research Funds for the Central Universities of China (JB2021043).

Competing Interests

The authors have no relevant financial or non-financial interests to disclose.

Author Contributions

All authors contributed to the study conception and design. Material preparation, data collection and analysis were performed by [Yulong ZHU]. The first draft of the manuscript was written by [Yafen ZHANG]. [Xiaoyu YAN], [Shu LI], [Qijing YU] and [Yidan WANG] contributed to data collection and all authors commented on previous versions of the manuscript. All authors read and approved the final manuscript.

References

1. Abraham MT, Satyam N, Rosi A, Pradhan B, Segoni S (2020) The selection of rain gauges and rainfall parameters in estimating intensity-duration thresholds for landslide occurrence: case study from Wayanad (India). Water 12(4):1000.
2. Chen CW, Saito H, Oguchi T (2015) Rainfall intensity–duration conditions for mass movements in Taiwan. Progress in Earth and Planetary Science 2(1):1-13.
3. Childs EC, Collis-George N (1950) The permeability of porous materials. Proc. R. Soc. Lond. A. Math. Phys. Sci 201:392-405.
4. Deng M, Chen N, Ding H (2018) Rainfall characteristics and thresholds for periglacial debris flows in the Parlung Zangbo Basin, southeast Tibetan Plateau. Journal of Earth System Science 127(1):1-17.
5. Fredlund MD, Wilson GW, Fredlund DG (2002) Use of the grain-size distribution for estimation of the soil-water characteristic curve. Can. Geotech. J 39(5):1103-1117.
6. GeoStudio International. GEOSLOPE, Calgary, Alberta, Canada, 2007.
7. Guo X, Cui P, Li Y, Ma L, Ge Y, Mahoney WB (2016) Intensity–duration threshold of rainfall-triggered debris flows in the Wenchuan earthquake affected area, China. Geomorphology 253:208-216.
8. Guzzetti F, Peruccacci S, Rossi M, Stark CP (2008) The rainfall intensity–duration control of shallow landslides and debris flows: an update. Landslides 5(1):3-17.
9. Jarosińska E (2018) An analysis of short duration high-intensity rainfall events in Cracow area. Infrastruktura i Ekologia Terenów Wiejskich 1(III): 575-588.
10. Jin Y, Ye L, Sun P (2021) Analysis and influence of rainfall infiltration of ancient city wall based on in-situ monitoring: a case study of The XingChun gate Lishui Prefecture. YANG JIN's personal collection (2021). 1 URL https://www.scipedia.com/public/Sun_JIN_2021a
11. Kim SW, Chun KW, Kim M, Catani F, Choi B, Seo JI (2021) Effect of antecedent rainfall conditions and their variations on shallow landslide-triggering rainfall thresholds in South Korea. Landslides 18(2):569-582.
12. Kuang X, Jiao JJ, Li H (2013) Review on airflow in unsaturated zones induced by natural forcings. Water Resources Research 49(10):6137-6165.

13. Larsen MC, Simon A (1993) A rainfall intensity-duration threshold for landslides in a humid-tropical environment, Puerto Rico. Geografiska Annaler: Series A. Physical Geography 75(1-2):13-23.
14. Marin RJ, Velásquez MF, García EF, Alvioli M, Aristizábal E (2021) Assessing two methods of defining rainfall intensity and duration thresholds for shallow landslides in data-scarce catchments of the Colombian Andean Mountains. Catena 206:105563.
15. Morgenstern NR, Price VE (1965) The analysis of the stability of general slip surfaces. Géotechnique 15:79-93.
16. Perera ENC, Jayawardana DT, Jayasinghe P (2017) A rainfall intensity-duration threshold for mass movement in Badulla, Sri Lanka. Journal of Geoscience and Environment Protection 5:135-152.
17. Rahardjo H, Lee TT, Leong EC, Rezaur RB (2005) Response of a residual soil slope to rainfall. Canadian Geotechnical Journal 42(2):340-351.
18. Richards LA (1931) Capillary conduction of liquids through porous mediums. J. Appl. Phys. 1.
19. Saito H, Nakayama D, Matsuyama H (2010) Relationship between the initiation of a shallow landslide and rainfall intensity-duration thresholds in Japan. Geomorphology 118(1-2):167-175.
20. Segoni S, Rossi G, Rosi A, Catani F (2014) Landslides triggered by rainfall: A semi-automated procedure to define consistent intensity–duration thresholds. Computers & Geosciences 63:123-131.
21. van Asch TWJ, Yu B, Hu W (2018) The Development of a 1-D Integrated Hydro-Mechanical Model Based on Flume Tests to Unravel Different Hydrological Triggering Processes of Debris Flows. Water 10(7):950.
22. Vanapalli SK, Fredlund DG, Pufahl DE, Clifton AW (1996) Model for the prediction of shear strength with respect to soil suction. Can. Geotech. J 33:379-392.
23. Zhang J, Huang HW, Zhang LM, Zhu HH, Shi B (2014) Probabilistic prediction of rainfall-induced slope failure using a mechanics-based model. Engineering Geology 168:129-140.
24. Zhu YL, Ishikawa T, Subramanian SS, Luo B (2020a) Simultaneous analysis of slope instabilities on a small catchment-scale using coupled surface and subsurface flows. Engineering Geology 275:105750.
25. Zhu YL Ishikawa T, Subramanian SS (2020b) Simulation of runoff and infiltration using iterative cross-coupled surface and subsurface flows. Japanese Geotechnical Society Special Publication 8 (3):41-46.

Figures

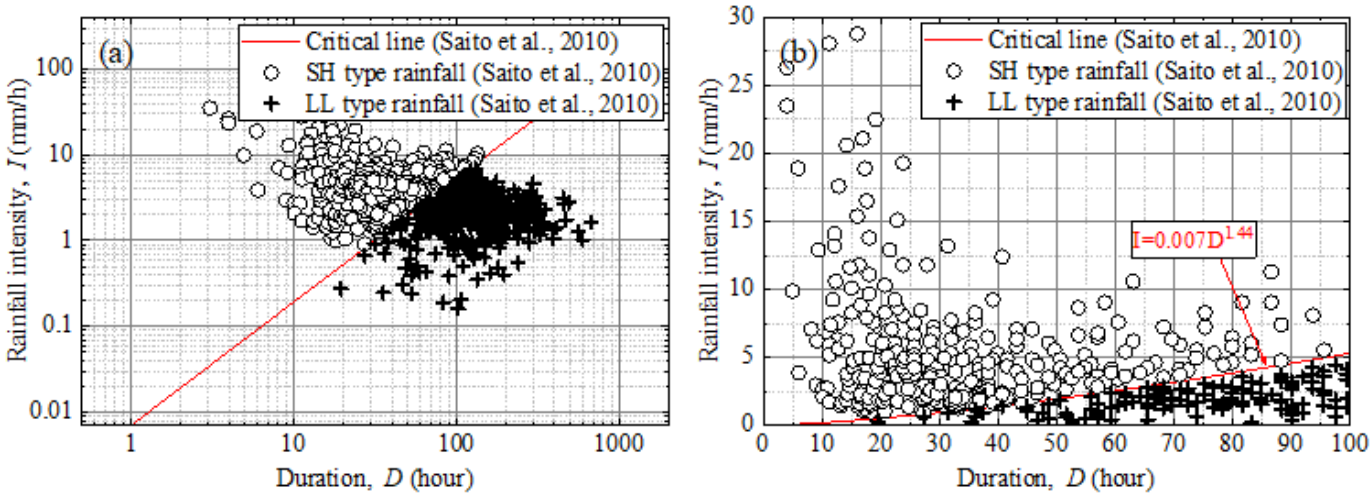

Figure 1

Classification of SH type rainfall and LL type rainfall by Saito et al. (2010). (a) logarithmic coordinates and (b) linear coordinates.

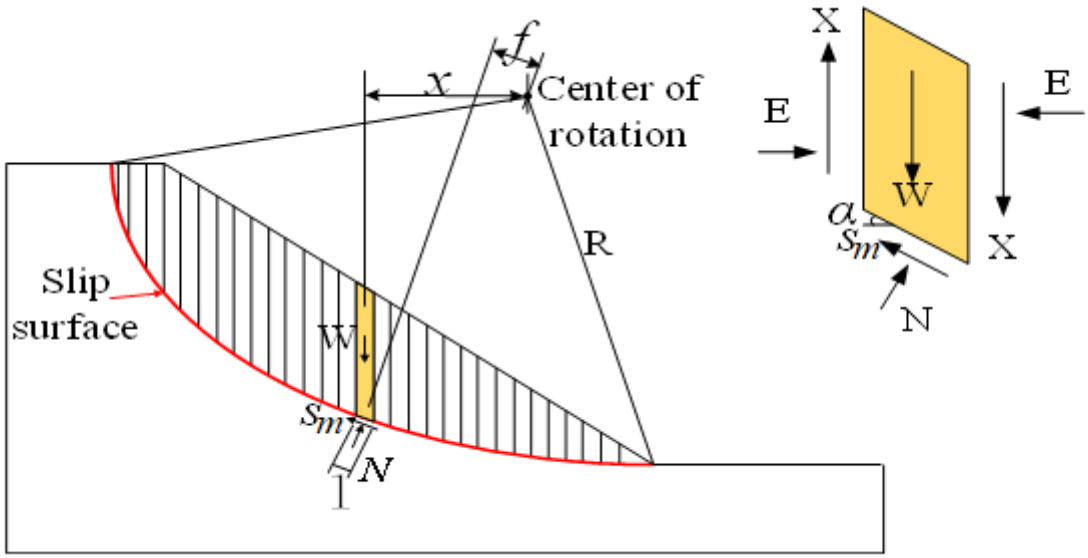

Figure 2

Slope stability was analyzed by the limit equilibrium method given by Morgenstern and Price (1965).

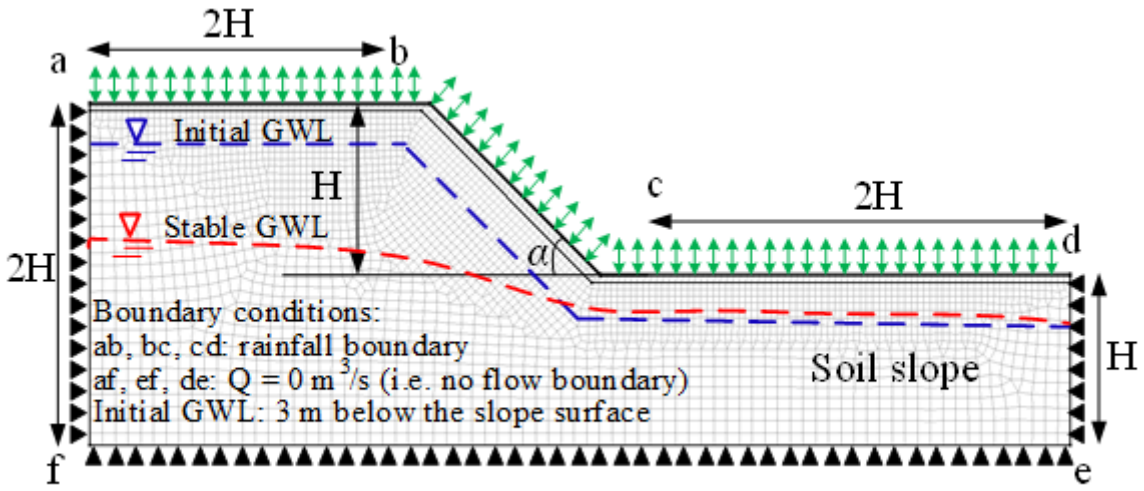

Figure 3

Homogeneous conceptual slope model with applied boundary conditions.

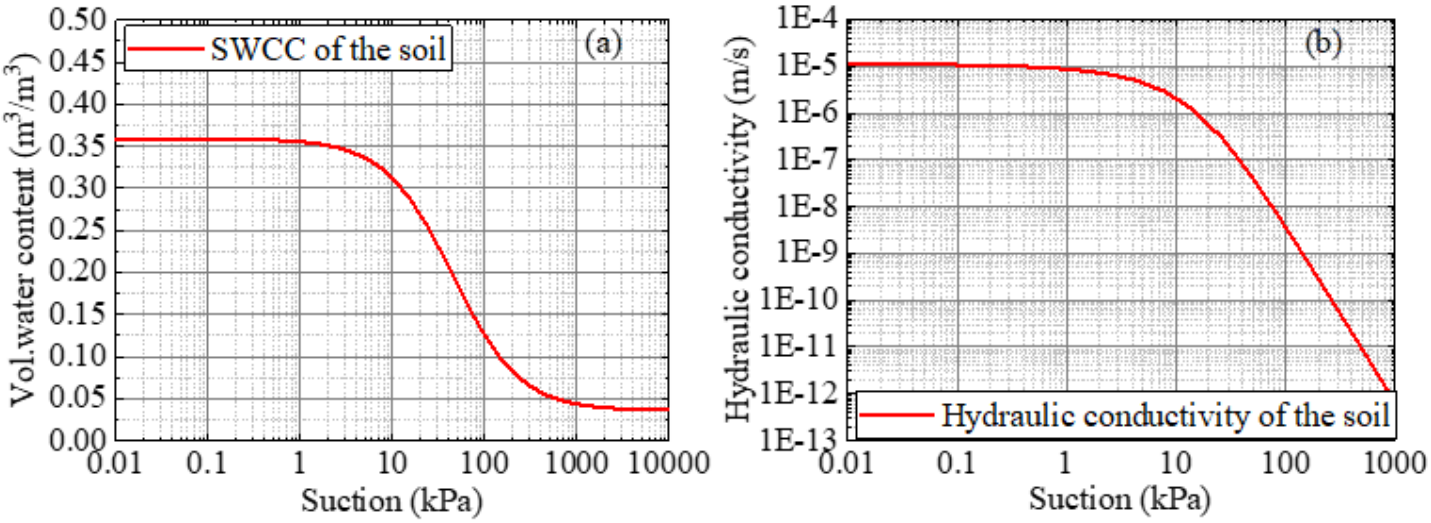

Figure 4

Soil water characteristic curve (SWCC) and hydraulic conductivity of the soil. (a) SWCC, (b) hydraulic conductivity.

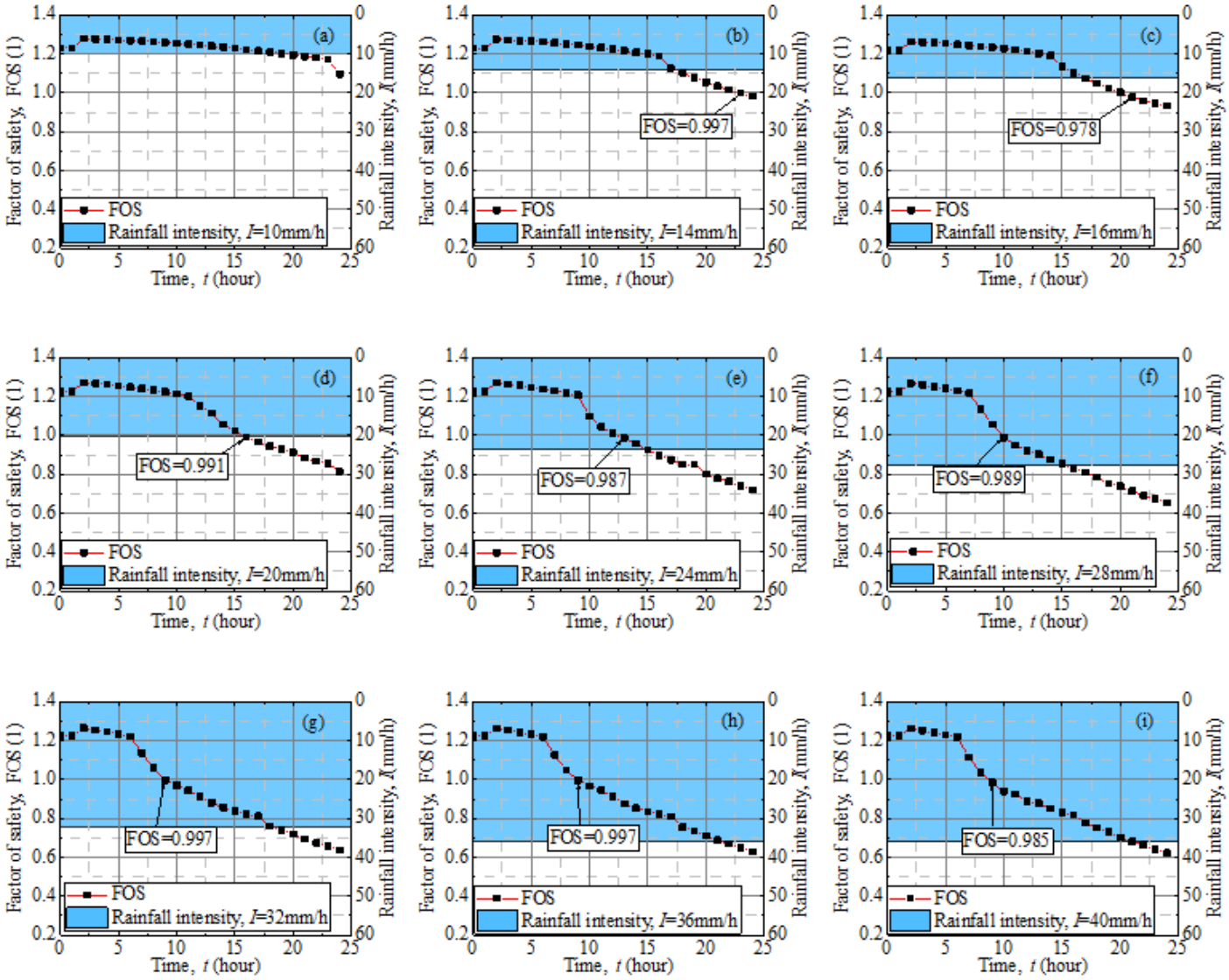

Figure 5

Factor of safety under different I-D conditions, (a) I=10 mm/h, (b) I=14 mm/h, (c) I=16 mm/h, (d) I=20 mm/h, (e) I=24 mm/h, (f) I=28 mm/h, (g) I=32 mm/h, (h) I=36 mm/h, (i) I=40 mm/h.

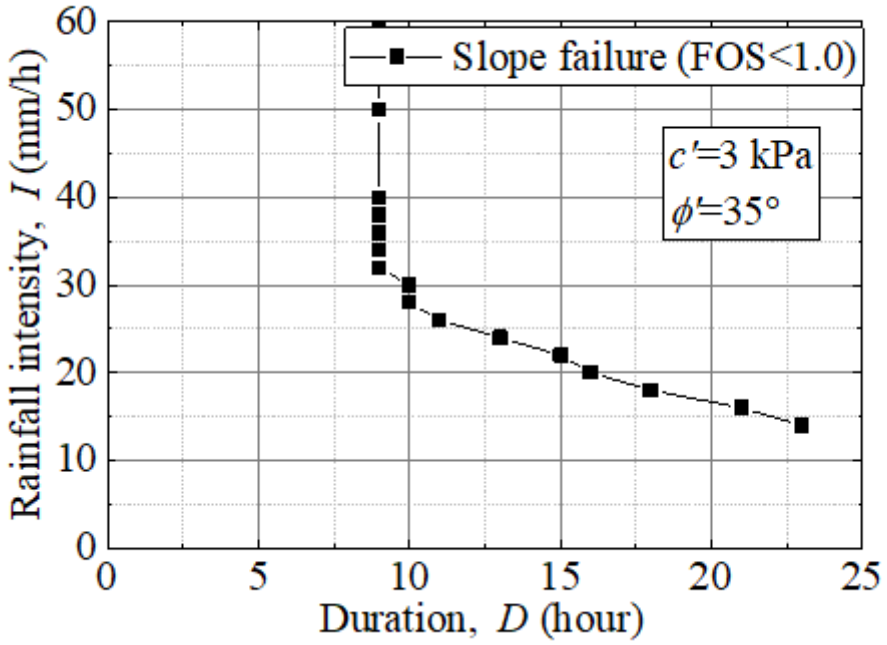

Figure 6

Threshold of slope failure in the I–D conditions 2D plane.

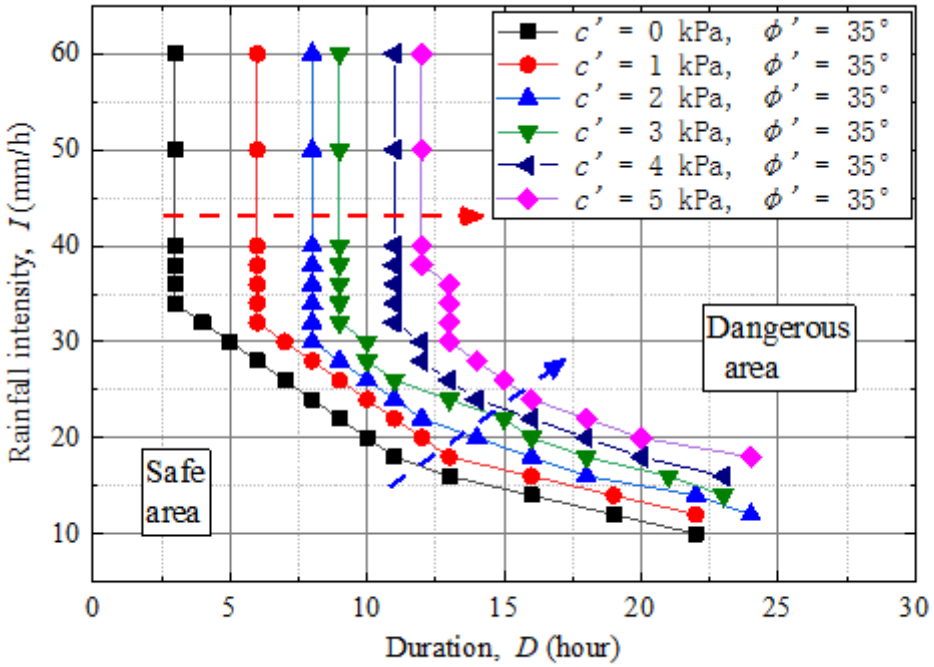

Figure 7

Thresholds of slope failure with different soil cohesion.

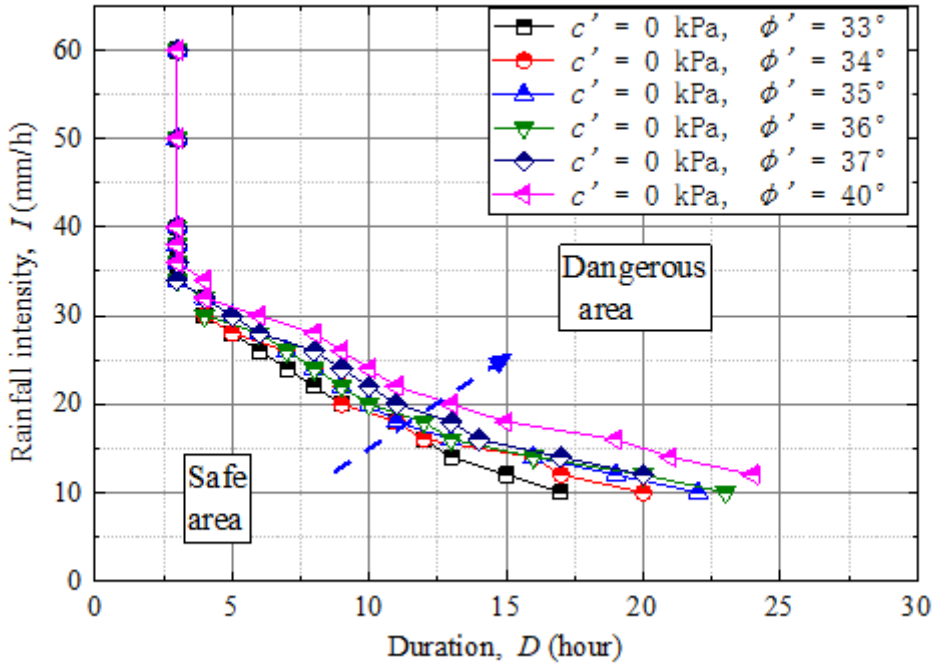

Figure 8

Thresholds of slope failure with different internal friction angles.

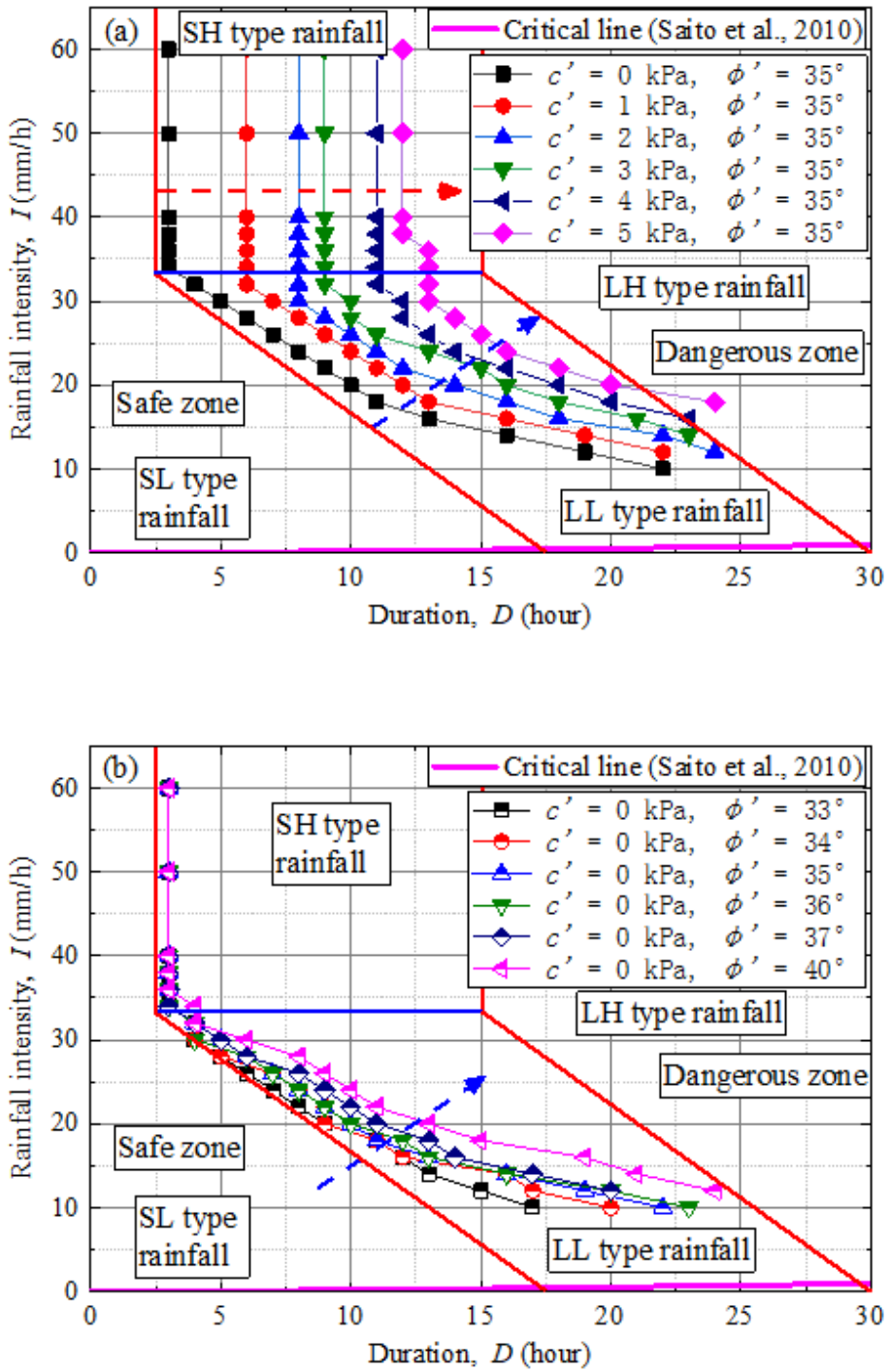

Figure 9

Classification of rainfall types based on slope instability with different soil properties (a) different cohesion and (b) different internal friction angle.

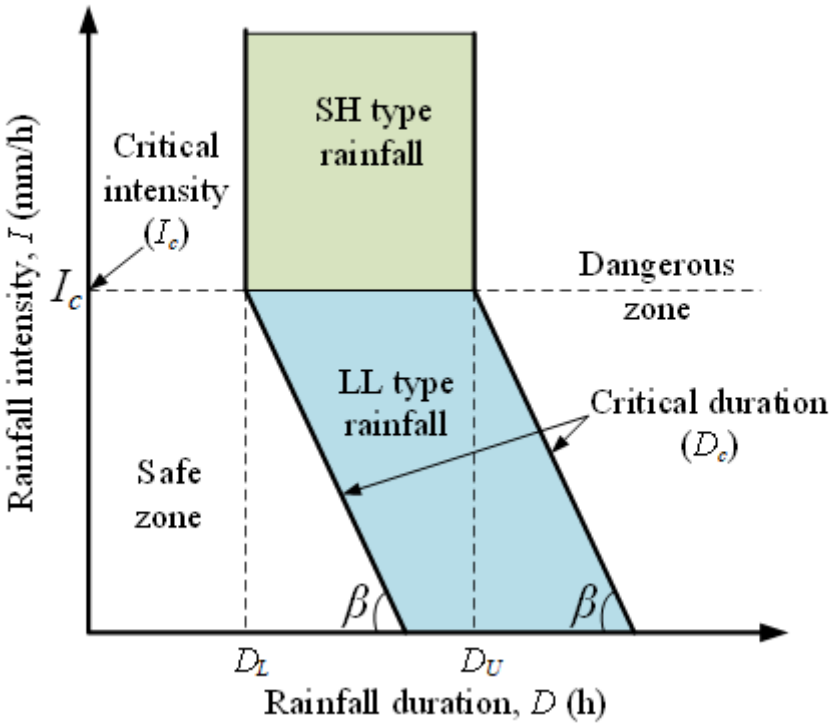

Figure 10

Proposal of the determination method of rainfall type.